Forest Ecology and Management 492 (2021) 119239

Contents lists available at ScienceDirect

Forest Ecology and Management

journal homepage: www.elsevier.com/locate/foreco

Detecting structural changes induced by Heterobasidion root rot on Scots pines using terrestrial laser scanning

Timo P. Pitkänen *, Tuula Piri, Aleksi Lehtonen, Mikko Peltoniemi

Natural Resources Institute Finland (Luke), Latokartanonkaari 9, FI-00790 Helsinki, Finland

ARTICLE INFO

Keywords:
Decay fungi
Forest stand management
Laser scanning
Point cloud data

ABSTRACT

Root rot, caused by the decay fungus *Heterobasidion annosum*, damages both below- and above-ground parts of Scots pines (*Pinus Sylvestris* L.). The diseased pines are often first characterized by deteriorated crowns and they will eventually be killed by the infection, but the process is gradual and difficult to be observed before the symptoms are severe. We tested the applicability of point cloud data produced by terrestrial laser scanning (TLS) for quantifying the structural differences between the healthy and the diseased trees. This approach was applied in a mature pine stand in southern Finland, which was known to be infected by *H. annosum*. We first scanned the stand using TLS, and thereafter felled the trees for detailed inspection and classification of the infection status. From the TLS point cloud, we estimated i) crosscut areas within the lowest 1 m of the stem, identifying potential deformations initiated by the fungus, ii) degree of crown deterioration, often providing the first visual signs of the infection at the level of individual trees, and iii) crown occupancy and open space around the trees, prone to be altered by the mycelial spread of the fungus between the adjacent trees. The results indicate that differences in both stem dimensions and crown deterioration can be detected between the healthy and the diseased trees. The diseased trees were found to have a more swollen butt, but no irregularities in circularity of the crosscuts were detected. In terms of vertical point distribution, the diseased trees had point accumulations at substantially greater heights, reflecting easier penetration of laser beams and sparsity of the crown. Regarding to crown occupancy, the diseased trees had more open space around their crowns, but difference to the healthy trees was not statistically significant. According to a simple prediction test based on the calculated features, up to 85% classification accuracy of the infection status was reached. This study is the first indication that TLS can successfully be applied for detecting structural changes of Scots pines connected to Heterobasidion root rot. Our results also show evidence that *H. annosum* causes butt swelling, which has rarely been reported as a symptom for Scots pines.

1. Introduction

Basidiomycete *Heterobasidion annosum* (Fr.) Bref. sensu lato is widely distributed over temperate conifer forests of the northern hemisphere causing a disease known as Heterobasidion root rot. Annual economic losses from Heterobasidion root rot are estimated to be 790 million euros in the EU region alone, excluding costs of controlling and diagnosing the disease as well as reduced resistance of the infected stands to storm damages (Gonthier and Thor, 2013; Woodward et al., 1998). Actually, *H. annosum* s.l. is a complex of *Heterobasidion* species with different host preferences. Among them, *H. annosum* sensu stricto is one of the most serious pathogens of pine forests in Eurasia. In addition to pine species, *H. annosum* s.str. causes root rot also on several other tree species, including deciduous trees (Garbelotto and Gonthier, 2013; Korhonen, 1978).

Heterobasidion spp. initiate primary infections via airborne basidiospores which can infect a freshly cut stump or wounded tree. From an infected tree or stump the fungus spreads vegetatively as mycelium through root contacts to the adjacent trees at a speed of up to 200 cm per year (Asiegbu et al., 2008; Garbelotto and Gonthier, 2013; Perttunen et al., 2013). Relatively short effective dispersal range of the spores may limit their spreading between forests, but *H. annosum* is capable of persisting for decades in the root systems of diseased trees, even after felling them (Greig and Pratt, 1976; Zaļuma et al., 2019). Therefore, the

* Corresponding author.
E-mail addresses: timo.p.pitkanen@luke.fi (T.P. Pitkänen), tuula.piri@luke.fi (T. Piri), aleksi.lehtonen@luke.fi (A. Lehtonen), mikko.peltoniemi@luke.fi (M. Peltoniemi).

https://doi.org/10.1016/j.foreco.2021.119239
Received 21 December 2020; Received in revised form 3 March 2021; Accepted 31 March 2021
Available online 29 April 2021

disease can be efficiently transmitted to the next tree generation planted on the respective site, and there is little chance to eradicate the fungus once it is firmly established in a stand (Garbelotto and Gonthier, 2013; Lygis et al., 2004; Piri, 2003). Due to mycelial spread, Heterobasidion root rot tends to cause tree mortality in patches rather than distributed at random, which may result in open areas up to 0.5 ha in case of the death of trees if no further actions are done (Lygis et al., 2004).

An infected pine secretes resin, which normally helps to keep the fungal infection within the root system and at the lowest part of the stem, i.e. up to a height of 30–40 cm (Laine, 1976; Wang et al., 2014). The existence of the fungus cause water stress and nutrient deficit due to root damage, which weakens the tree and lowers its resistance to other pests and pathogens over the time. This will increase the likelihood of further fungal diseases or attacks of bark beetles, and finally causes a premature death of the diseased tree (Alexander, 1980; Jankowiak and Rossa, 2008; Otrosina, 1997; Piri, 2000). Heterobasidion root rot will also gradually initiate a range of externally visible symptoms, including crown thinning and transparency, exudation of resin, reduction in terminal growth, and slight swelling of the butt part (Asiegbu et al., 2008; DeNitto, 1989; Kurkela, 2002; Laine, 1976). Obvious butt swelling, however, is principally associated to spruces, and to our knowledge there is no measure-based evidence of butt deformations regarding to pines.

The challenge in detecting the root rot is that a diseased mature pine appears externally almost intact for decades, until up to 30% of the roots are infected (Byler, 1989; Kurkela, 2002; Wang et al., 2014). For this reason, observing and quantifying external symptoms at the level of individual trees is challenging and unreliable, leading easily to a belated discovery and underestimated severity of the problem (Rönnberg et al., 2006). The fungus is however capable of infecting and killing seedlings and young trees at much faster rate, which may be destructive for the next tree generation, and provide virtually no other management alternatives than planting less susceptible deciduous species on an infected site (Laine, 1976; Swedjemark and Stenlid, 1995; Werner and Łakomy, 2002). Decisions on stand management are however often made based on visual judgement of root rot damage but in reality, the number of diseased trees that appear healthy may be up to three times larger than the number of clearly degraded or dead trees (DeNitto, 1989; Kurkela, 2002).

The primary method for preventing *Heterobasidion* infections is to treat freshly cut stumps with biocontrol or chemical control agent to stop basidiospore germination (Johansson et al., 2002; Nicolotti et al., 1999; Varese et al., 2003). In infested stands, prevention is too late, and management actions can only minimize the immediate economic losses without efficiently inhibiting the further spread. Reliable identification of the infected trees however provides a better opportunity to harvest them before the decrease of their commercial value due to secondary damages (windthrow, attack by bark beetles, or discoloration by blue stain fungi). Moreover, early detection of root rot and magnitude of the problem would also help to assess future forest management strategies, e.g., choice of tree species for the next stand rotation – especially in stands with incipient root rot and small number of visibly identifiable infected trees.

As external and structural changes due to root rot are gradual but inevitable, improvements in measuring technique could potentially assist in their earlier detection. One promising recent technology for measuring and characterizing trees is terrestrial laser scanning (TLS), which enables non-destructive acquisition of a dense 3D point cloud at a millimeter-level accuracy. Forest-related use of TLS was initially focused on improving the efficiency of relatively simple measurements, such as tree positions and their diameters, but gradually the range of applications has shifted towards more complex features which are important but not directly measurable, including leaf area index, canopy details, full-tree volume, and various biomass fractions (Disney et al., 2019; Liang et al., 2016; Malhi et al., 2018; Saarinen et al., 2017). Increasingly, TLS-derived studies have also focused on structural details and anomalies of single trees, such as quantifying stem profile properties (Olofsson and Holmgren, 2016; Puletti et al., 2019), detecting effects of competition on tree growth and crown structure (Barbeito et al., 2017; Metz et al., 2013; Seidel et al., 2011), and reconstructing detailed branch architectures (Boudon et al., 2014; Li et al., 2020; Pyörälä et al., 2018). TLS data has also been applied to indicate canopy defects on oil palms due to basal stem rot, caused by the *Ganoderma* fungus (Azuan et al., 2019; Husin et al., 2020; Khosrokhani et al., 2018), but to our best knowledge not for detecting any other fungal infections with trees.

The objective of the study was to test the capabilities of TLS data to be used for identifying the root rot (*Heterobasidon annosum* s.str.) infected and healthy Scots pine (*Pinus sylvestris* L.) individuals. For this purpose, we first scanned a forest stand known to be infected by root rot using a terrestrial laser scanner. From the respective stand, we selected 30 Scots pines including externally healthy and diseased trees, which were felled down, inspected in detail regarding to any signs of the root rot infection, and determined whether they were predominantly healthy or not. Then, we used the TLS-derived point cloud to find evidence on potential butt deformations by measuring stem cross-sections, identify crown deterioration by vertical penetration of laser beams, and quantify stand openness with consequently altered canopy competition. These results were compared between the healthy and the infected individuals, aiming at to verify the range and the magnitude of structural changes with implications on improved root rot detection and management of the infected stands.

2. Materials and methods

2.1. Study area and fieldwork

Fieldwork for the study was conducted in Haapastensyrjä research forest, Southern Finland (Fig. 1), on a Scots pine monoculture stand planted on a relatively fertile soil and later got infected by *H. annosum* s. str. Initially, the stand had been established for studying forest genetics through a progeny trial of phenotypically selected parents, similarly as described by Ruotsalainen (2014), thus resulting in all the studied trees to be siblings with each other with limited genetic variation. Part of the trees in the stand expressed various visible symptoms with potential connection to *Heterobasidion* infection, ranging from individuals with slightly deteriorated crowns to totally dead trees. It should however be noted that the site was initially known to be infected and thereafter carefully evaluated by a group of professionals, thus primarily reflecting a stage when a random, mature Scots pine stand would gradually start to be under suspicion of root rot. From this stand, altogether 30 sample trees were selected, including both trees expected to be suffering from root rot, as well as visually healthy-looking trees. These trees were scanned in May 2019 and felled in October 2019.

Location, diameter at breast height (1.3 m; DBH), height of the living crown base (h_C) and tree height (h_T) were first measured from standing sample trees. The trees were also marked with duct tape at h = 1.4 m, thus assisting their later identification and providing a reference height for TLS analyses. Scanning was performed using Leica P40 time-of-flight scanner, having $<$ 0.23 mrad beam divergence and $\leq$ 3.5 mm beam diameter at front window, and offering a 3D position accuracy of 3 mm at 50 m distance. Scanning stations (9) were positioned so that each sample tree was confirmed to be visible from more than one station, and from several directions. Five spheroid targets were set around the plot for co-registration, of which at least three were visible to each station. Scans were made using a 3.1 mm point spacing at 10 m distance and co-registered at an average error of 0.8 mm. Weather during the scanning was dry with light wind and 15 °C temperature.

After scanning, the sample trees were felled and the stump surface of each tree was inspected visually for signs that referred for *Heterobasidion* infection, i.e. decay and resinous patches. Moreover, 1–2 wood samples were taken with the aid of an increment borer from the butt of each sample tree to ensure possible *Heterobasidion* infection. Wood samples

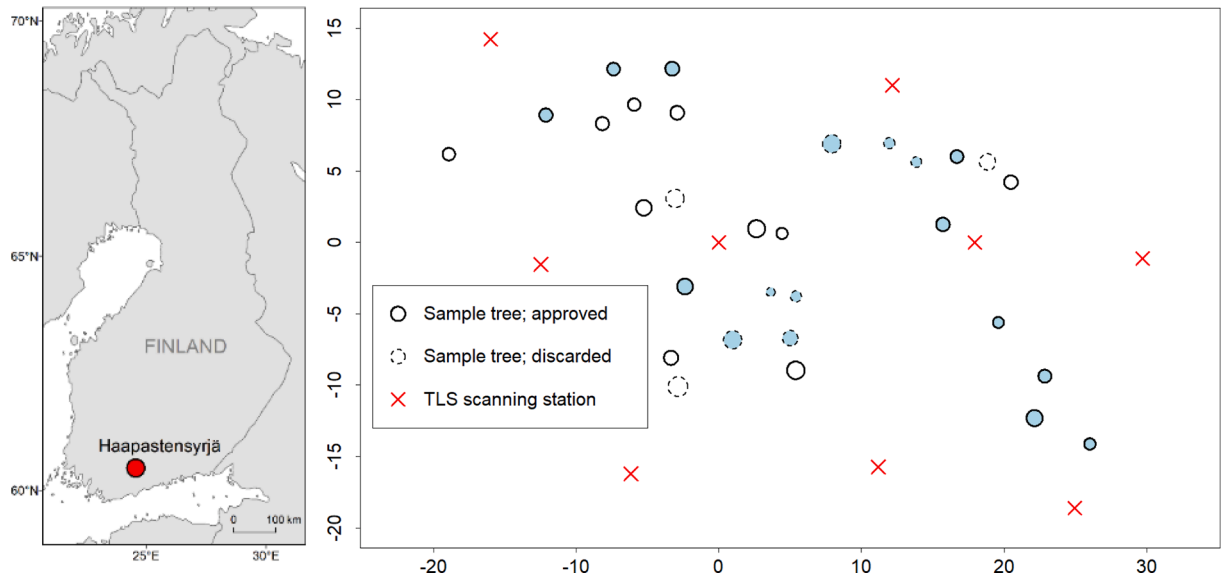

Fig. 1. Location of the study site (left) and positions of the sample trees (right). Trees have been visualized using 5× factor as compared to their measured DBH. Diseased trees are shown with light blue background color, and coordinates (in meters) are relative to the location of the first scanning station (0,0). Further details are explained in the text. Background map: © EuroGeographics for the administrative boundaries. (For interpretation of the references to color in this figure legend, the reader is referred to the web version of this article.)

were cultured on malt agar (2% MEA) and after 5–7 days incubation the presence of *Heterobasidion* mycelia growing out of the wood samples was examined under a dissection microscope. Finally, based on the visual estimation of tree crown and stump surface and analyses of wood samples, the trees were classified into healthy and diseased ones, and, further, the diseased trees into four categories based on the degree of the decay at stump level: trees with discoloration (presence of *Heterobasidion* infection probable but uncertain), incipient decay, distinct decay, and advanced decay.

Of the 30 sample trees, 13 were assessed healthy and 17 diseased, and separated into their respective groups. The two groups differed in terms of tree dimensions (DBH and h_T) with potential consequences to the results. To balance them, only trees with DBH between 150 and 250 mm, and height of 20 m or less, were approved (n = 23). Further, the diseased individuals categorized as discolored or with incipient decay (n = 3) were removed as their correct classification was regarded as most uncertain, and external changes the least expressive of root rot. Applying these conditions resulted in the final approval of 20 sample trees at equally sized groups, which were further compared by the distributions of their DBH, h_T and form factor (f) for indicating any obvious differences. Form factor refers to total stem volume divided by a volume of a cylinder, with diameter equaling the measurement at breast height (Van Laar and Akça, 2007):

$$f = \frac{v_S}{g \times h_T} \tag{1}$$

where v_S is the total stem volume as calculated using volume equation of Laasasenaho (1982), g is basal area at breast height, and h_T tree height, respectively. Form factor was included to indicate potential stem form differences which cannot be interpreted based on only DBH and h_T distributions. Comparison was performed using box-plot diagrams, as any further statistical analyses were expected to have low power for any meaningful inferences due to the limited sample size.

2.2. TLS processing and analysis of stem deformations

For TLS-based measurements, sample trees were manually extracted from the co-registered TLS data into individual point clouds using Leica Cyclone 9.1 software. Tree points were then automatically fitted as cylinders to construct the stem similarly to Pitkänen et al. (2019), and these cylinders were used at later stages for defining the stem location. To provide accurate information on potential deformations related swollen or non-round sections near to the stem base (i.e., the ground level), however, the stem edge was extracted manually from the point cloud instead of using the fitted cylinders. This was performed at 20 cm intervals between the heights of 20 cm and 100 cm as detectable deformations, if any, were expected to be close to the stem base. Detection of stem edge was generally impossible below the height of 20 cm due to heavily occluded point cloud resulting from ground vegetation.

For each tree and analyzed height, TLS points were extracted within ± 5 cm vertical distance around the respective height, and converted into a two-dimensional (flattened to x,y plane) raster image. This raster was used to digitize the stem edge manually with ArcMap 10.6 software, thus enabling the calculation of its cross-section area. Then, the tree-wise cross-section areas at different heights were divided to calculate their pairwise ratios. And further, all the respective ratios were compared between the two groups (i.e. the healthy and the diseased trees) using a two-tailed t-test, to indicate potential tapering differences between the measured heights. Applying a manual stem extraction method instead of automatized approaches derived principally from our particular interest in the tree butts, which suffered from occlusions due to undergrowth. Additional advantage of manual stem extraction was the ability to assess stem circularities (as presented below). Occluded data with potential outliers allows primarily only the use of circle- or cylinder-based fitting approaches, which have no capabilities to indicate asymmetry.

Further, circularities of the cross-sections were evaluated as it was unknown whether the infection would cause changes in the stem symmetricity. For this purpose, every extracted cross-section was calculated a root-mean-square deviation (RMSD), indicating the difference between the digitization node distances (start or end of a single line segment) from the stem center as compared to the reference distance, i.e., the radius of a circle equaling the cross-section area:

$$RMSD = \sqrt{\frac{\sum_{n=1}^{N} (d_n - r)^2}{N}} \tag{2}$$

where N is the total number of nodes, d_n is the distance of the node n to

the stem center, and r is the reference distance. Then, the RMSD value distributions of each cross-section height were compared between the healthy and the diseased trees using Mood's median test, which was selected as a more robust and nonparametric alternative for t-test. Comparison of the symmetricities could have also been done using simpler area/perimeter ratio, but it was regarded as being more sensitive to bark roughness and other minor deviations, which were not the targeted differences in this context.

2.3. Assessing crown deterioration

Detection of crown differences between the healthy and the diseased trees was based on vertical distribution of TLS points. As the number and coverage of TLS points depend on the location of scanning stations and visibility of the sample trees from them, it was first confirmed using two-sample Kolmogorov-Smirnov test that the station distances of the two groups with respect to the sample trees were not significantly different (i.e. affecting the expected point densities). Regarding to tree visibilities or vertical coverage of TLS points, no specific statistics could be calculated, but rationality in the field-based station assignments was expected to ensure sufficient similarity between the groups.

Vertical TLS point distribution was calculated by proportioning each z-coordinate to the h_T of the respective tree. Even though the main interest was in the crown part, stem points below h_C were not removed, as the location of the living crown base potentially depended on the level of infection, and thus it was appropriate to include lower but dead branches in the analysis. Then, two-sample Kolmogorov-Smirnov test was used to indicate whether the vertical point distributions of the two groups differed from each other, followed by visualizing the distributions using binned and cumulative histograms for more detailed interpretation.

Further, to observe potential dependencies of butt swelling and crown deterioration, the median z-coordinate of each tree-wise point cloud as proportioned to h_T were compared to the previously calculated cross-section area ratios with most significant differences between the healthy and the diseased trees. Median z-coordinate was expected to provide a simple but applicable indictor of crown deterioration, located normally within the lower part of the crown but shifting upwards according to easier penetration of TLS beams into the crown layer. The dependencies were then tested for linear correlation using Pearson's product-moment correlation as well as visualized in a plot.

2.4. Quantifying crown occupancy

As root rot has been reported to cause crown deterioration and, ultimately, death of the diseased trees (Greig, 1998), it was investigated whether the infected parts of the stand would be characterized by sparser canopy density. Secondly, we wanted to know whether the crowns of the diseased and healthy trees were differentially impacted by peer competition. To support these analyses, we calculated the proportion of empty space around the crowns, larger values indicating reduced presence of neighboring tree crowns. Space occupied by the sample tree crowns and existence of competing tree crowns in their immediate vicinity were calculated similarly to Martin-Ducup et al. (2016) and Seidel et al. (2015), using an upside-down cone with a 60° opening angle, which was placed at the crown base. This so-called search cone approach provides a relatively straightforward method with TLS data for identifying competitors and their pressure to the targeted tree, expecting that surrounding trees with intersecting crown parts will cause competition pressure (Metz et al., 2013).

All sample trees had been measured their crown base, which were calculated relative to h_T. According to two-tailed t-test, however, crown base of healthy trees was significantly ($p = 0.04$) lower. To avoid any bias deriving from these differences, crown base was decided to be defined at 55% relative height for all the sample trees. This corresponded to previous knowledge on the crown height of mature Scots pines in similar conditions (Hynynen and Saramäki, 1995), and was very close to the mean value of all sample trees.

For each sample tree, the upside-down cone was set at 55% relative height with upper limit at the h_T and divided into $0.1 \times 0.1 \times 0.1$ m voxels. Each voxel was first checked using the individual tree cloud and stored whether it was occupied (i.e. at least one TLS point) or empty by the respective tree. Then, a similar check was conducted using the full co-registered point cloud, providing information on voxels which were empty by the sample tree, but occupied by a potential nearby competitor. Based on this information, three indicators of crown occupancy and competitor pressure were calculated: 1) proportion of the cone filled by the sample tree; 2) proportion of the cone filled by potential competitor trees; and 3) proportion of the cone filled by any tree. These results were expected to provide simple but applicable measurements related to the spatial crown occupancy and applied to compare the two groups using one-tailed t-tests, i.e., testing whether the infected trees had sparser canopy density or not.

2.5. Predicting infection status

Finally, a simple leave-one-out prediction test was performed to assess the capabilities of the TLS-derived statistics to classify an unknown tree as a healthy or a diseased individual. For this purpose, three previously calculated indicators were selected:

(1) the pairwise cross-section area ratio with proportionally the largest mean difference between the two groups, to express potential variation in the stem form;
(2) the relative median z-coordinate of the tree-wise point cloud, to quantify the point distribution pattern and potential crown deterioration; and
(3) the proportion of point-filled voxels (by the target tree or any other tree) within the applied search cone, to indicate local differences in the canopy density.

All the indicators were scaled between 0 and 1 (min-max), each tree was left out in turn, and median values of the healthy and the infected trees were calculated based on the remaining trees. Then, for all the individual indicators as well as their combinations, the excluded tree was classified either healthy or diseased according to the closest median. In case several indicators were included, this classification was based on Euclidean distances in 2D/3D space to the points defined by the median values. Finally, the proportion of correct class assignments for each applied indicator and their combination were calculated.

3. Results

3.1. Characteristics of the sample trees

As indicated in Fig. 2, the characteristics of the healthy and the diseased trees were not exactly identical, but the observed differences were considered minor and all the median values were relatively similar between the two groups. Visual evaluation of the trees (Fig. 3) also indicated no obvious structural bias or defects which would be expected to increase differences between the healthy and the diseased trees.

3.2. Stem deformations

The mean cross-section areas of the healthy trees are generally larger (Table 1), as resulting from their slightly bigger average size, but median values of the diseased tree exceed their healthy counterparts at the heights of 20 and 40 cm. This suggests the diseased trees to have individuals with substantially swollen butts, which is indicated by the pairwise ratios as well (Table 2). The largest proportional difference was found between the heights of 20 and 80 cm, which was therefore selected as an indicator for the class prediction (chapter 3.5). In terms of

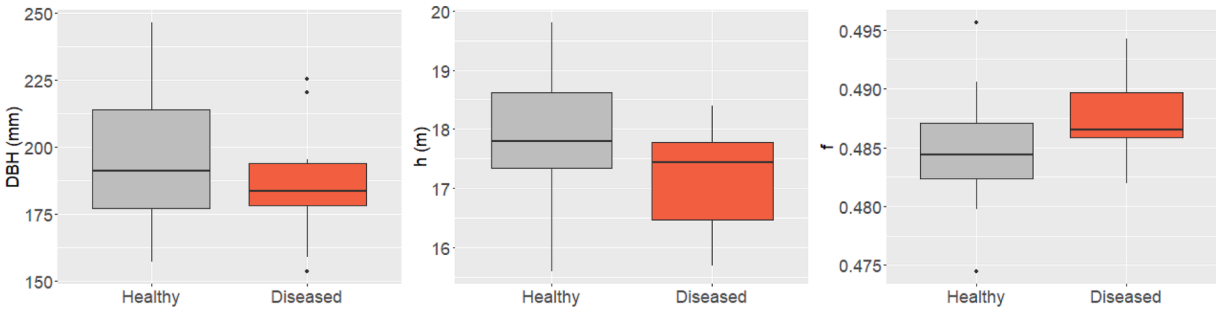

Fig. 2. Distributions of DBH, h_T and f of the healthy and the diseased trees, indicating the median value (horizontal line), the first and third quartiles (lower and upper hinges), and the value range (whiskers and outlier values, the latter defined as locating further than 1.5 * interquartile range from the respective hinge).

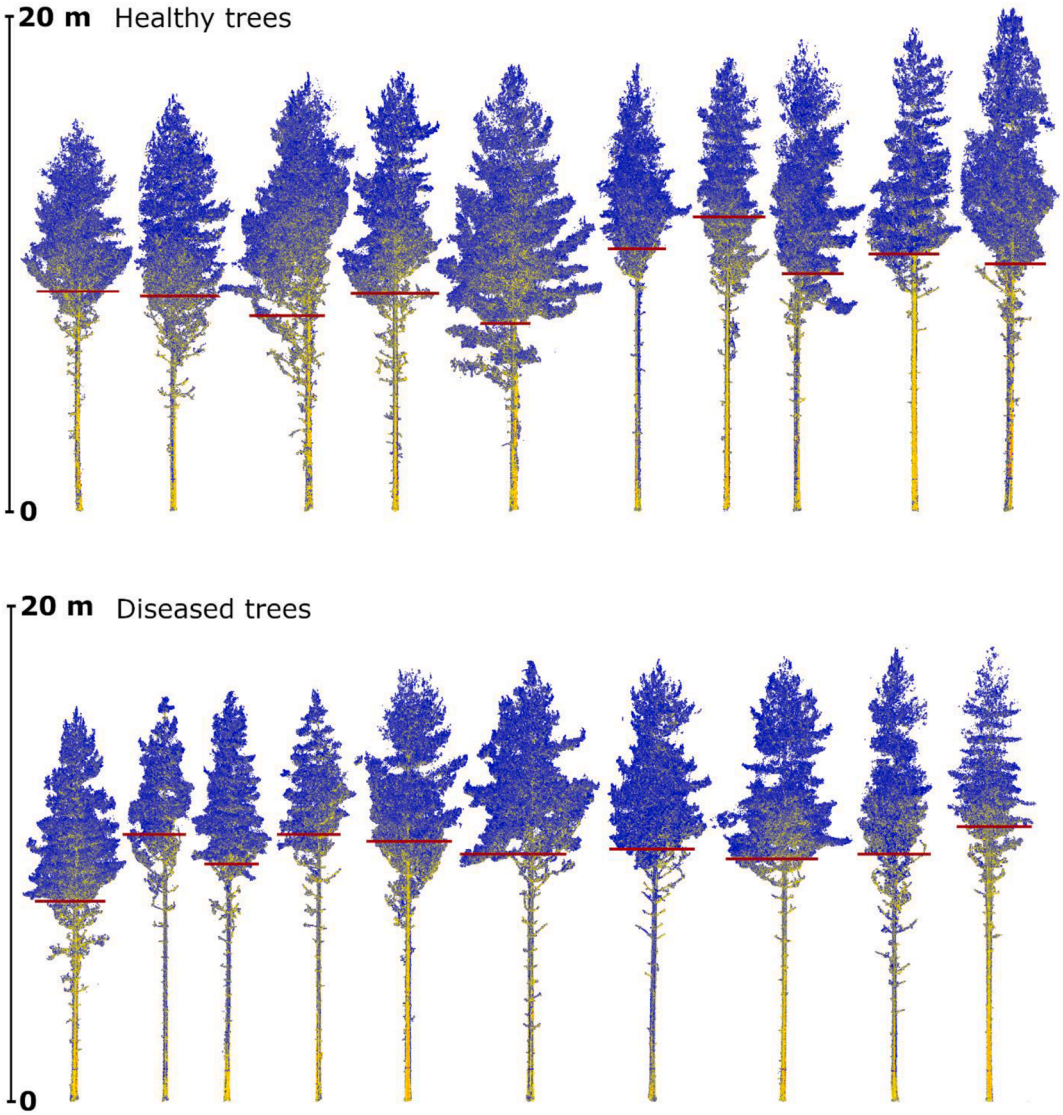

Fig. 3. The extracted sample trees, visualized by colors indicating backscattered beam intensities (red = high, blue = low) as registered by the TLS scanner. Field-measured h_C values are indicated by red horizontal lines. (For interpretation of the references to color in this figure legend, the reader is referred to the web version of this article.)

statistical significance, the two groups differed from each other when cross-sections on the heights of 20 cm or 40 cm were compared to any of the upper cross-sections at h = 60–100 cm. Given the presence of multiple tests, applying the rather conservative Bonferroni correction would retain only the statistical significance of comparing the heights of 40 and 80 cm.

Regarding to the cross-section circularities, Mood's median test showed no significant differences between the healthy and the diseased trees with p values ranging between 0.60 and 0.86, therefore providing no evidence of root rot induced irregularities near to the stem base.

Table 1
Mean and median (in brackets) values of digitized cross-section areas (cm^2) for healthy and diseased trees at different heights.

	20 cm	40 cm	60 cm	80 cm	100 cm
Healthy trees	455.9 (411.5)	405.2 (355.0)	380.9 (343.1)	362.0 (317.8)	343.3 (303.5)
Diseased trees	437.0 (440.0)	371.4 (361.0)	336.2 (319.6)	314.7 (295.2)	299.0 (287.8)

3.3. Crown deterioration

Vertical point distributions of the healthy and the diseased trees were significantly different with a p-value of < 0.01. Principal differences can be seen from point distributions (Fig. 4), containing all the TLS points of the respective groups as proportioned to h_T. The healthy trees have a considerably longer crown, whereas the diseased trees have a shorter crown concentrated on the topmost part the stem. Healthy trees also include a few obvious point accumulations (peaks) below the more continuous crown part derived from lush branches at lower heights, whereas diseased trees are lacking these features. Similar tendencies are apparent from both absolute as well as cumulative point distributions.

When median z-coordinate values of TLS points (as proportioned to h_T) were compared to cross-section area ratios with the highest difference between the groups (h = 40 cm/80 cm), no significant linear correlation between the butt swelling and crown deterioration was found either at the level of the whole data, or within the two groups (Fig. 5). In spite of this, the diseased trees stood out from the healthy individuals: diseased trees had either a markedly swollen butt or exceptionally high median z-coordinate, i.e. expectedly deteriorated crown, but only in few cases both.

3.4. Crown occupancy

On average, diseased trees occupy smaller proportion of the cone, experience less competitor pressure, and have altogether more space around their crowns (Table 3). The differences can be interpreted as marginally significant, but none of the differences between the two groups are significant at the level of p = 0.05.

3.5. Class prediction

Of the selected predictors (Fig. 6), the median z-coordinate of the point cloud had the highest single-indicator prediction power (75%), while the voxel proportion (55%) had hardly any effect as compared to the expected success of random class assignments (50%). The results of data combinations are somewhat mixed; while the voxel proportion

Table 2
Mean cross-section area ratios of comparing lower to higher diameters for healthy (a) and diseased trees (b), and significance (p-values) of the differences between the two groups (c). For p-values, significant ($p < 0.05$) are indicated in red and bolded, and marginally significant ($0.05 \leq p < 0.1$) in blue and italicized font, as interpreted at the level of individual tests.

a. Healty trees

	40 cm	60 cm	80 cm	100 cm
20 cm	1.124	1.194	1.261	1.327
40 cm		1.063	1.122	1.181
60 cm			1.056	1.111
80 cm				1.052

b. Diseased trees

	40 cm	60 cm	80 cm	100 cm
20 cm	1.181	1.301	1.393	1.463
40 cm		1.101	1.179	1.238
60 cm			1.070	1.124
80 cm				1.051

c. Significance of differences

	40 cm	60 cm	80 cm	100 cm
20 cm	*0.088*	**0.023**	**0.015**	**0.013**
40 cm		**0.010**	**0.005**	**0.013**
60 cm			0.216	0.335
80 cm				0.889

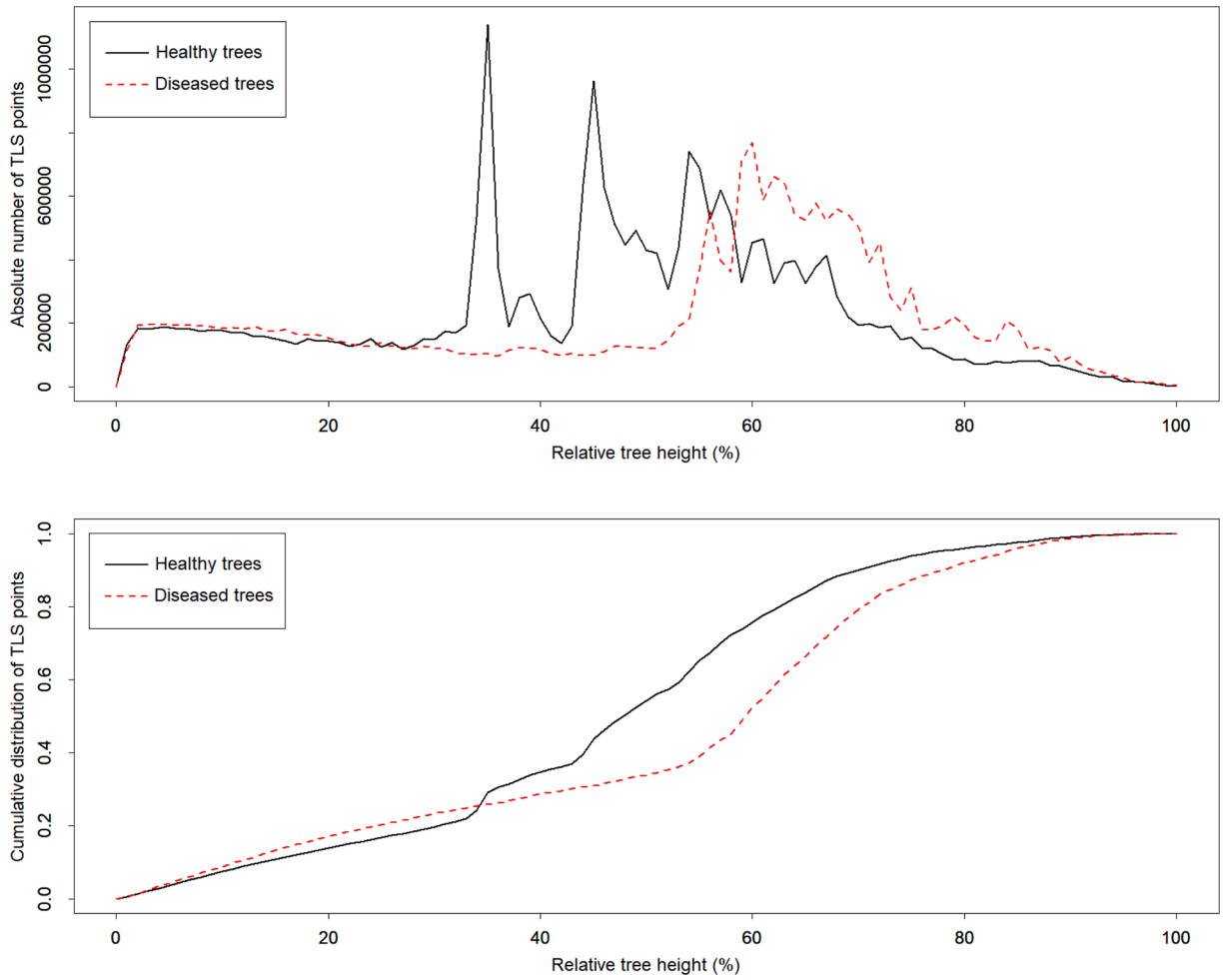

Fig. 4. Vertical TLS point distributions of the healthy and the diseased trees, presented using absolute point numbers in 1% bins (above) as well as cumulative histogram (below).

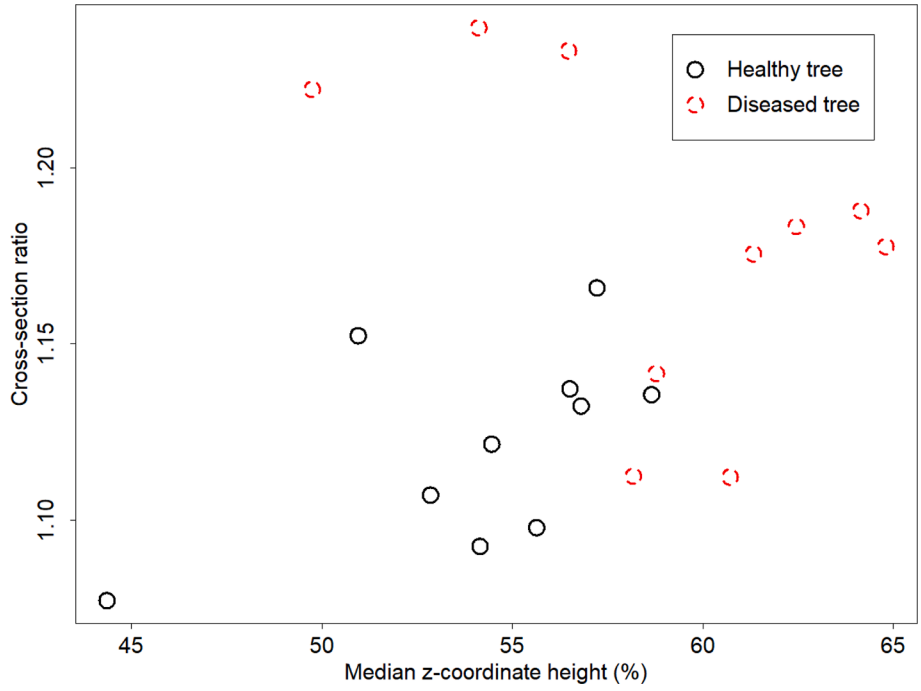

Fig. 5. Tree-wise median z-coordinate values of TLS points plotted against cross-section area ratios, as calculated between the heights of 40 and 80 cm.

Table 3
Average occupancy proportions within the search cone, divided into healthy and diseased trees, and significance of the differences between the two groups according to the one-tailed *t*-test.

	Sample tree	Adjacent trees	All trees
Healthy	5,30%	5,71%	11,01%
Diseased	4,44%	4,54%	8,97%
p-value	0,083	0,200	0,086

improves the performance of the cross-section ration, the effect is opposite when combined with the median z coordinate. The best result of 85% accuracy, or 17 correctly classified trees out of 20, was achieved by combining the cross-section ratio with the median z-coordinate, regardless if the voxel proportion was included or not. Given the small number of instances, however, effects of random deviation of the target trees and their respective indicator values may be relatively high.

4. Discussion

Heterobasidion infection will be destructive for a forest stand and complete eradication of the fungus is virtually impossible, unless replacing the susceptible tree species by a more resistant one. Thus, actions for minimizing its effects should concentrate on preventing new infections and keeping damage at the lowest possible level in already infected stands. Our study presents measurements from a single stand, but given the similarities in the site conditions and genetic background of the trees yet differences found between the healthy and the infected individuals, the results underline the applicability of point cloud data for quantifying the impacts of Heterobasidion root rot. This demonstrates that data from terrestrial laser scanning can provide substantial assistance for detecting the diseased trees by their structural characteristics, therefore offering information for minimizing the infection-derived economic losses and supporting targeted forest management.

According to the results, trees suffering from root rot are characterized by a more swollen butt, which tapers relatively quickly to normal dimensions between the heights of 0.4–0.6 m as compared to healthy trees. This may at least partially derive from increased secretion of resin, which is affecting primarily the lowest 30–40 cm of the stem for matured pines (Laine, 1976). Although statistically significant differences of the cross-section ratios were found between the healthy and the diseased trees, the observed differences were relatively small in terms of the absolute dimensions. This probably also explains why butt swelling has not been considered as a normal symptom of Scots pines. As such, TLS-derived measurements are capable of indicating such minor differences, but this sets high requirements for the data analysis and its potential automatization. Non-circularity or any obvious irregularities of the stem butt, however, do not appear to provide any additional information for finding the infected trees.

Analysis based on the vertical distribution of TLS points indicates that healthy trees have denser and longer crown structure, which reflects the laser beams from lower relative heights as compared to trees suffering from root rot infection. Healthy trees also appear to have lush branches below the continuous crown more frequently than diseased ones, as indicated by lower peaks in the histograms of Fig. 4. Higher concentrations of points of the diseased trees may be partially due to better visibility of the crowns with respect to larger empty space around them. However, the obviously different vertical point distribution patterns are suggesting that these tendencies are more likely resulting from structural differences of the respective trees. Therefore, we consider that the crown shape differences likely derive directly from the root rot infection and its damages for the root system and sapwood, causing needle loss and decreasing crown density (Kurkela, 2002; Laine, 1976). Causalities are, however, not always straightforward, as crown deterioration may also results from various other reasons than root rot. Frequently, simultaneous attacks by various other pathogens or insect pests which will increase the severity of the symptoms have been observed (Bonello, 2008; Eyles, 2007; Kolosova and Bohlmann, 2012). Therefore, while crown deterioration is known to be associated to root rot, its existence or magnitude cannot be used as a sole indicator of *Heterobasidion* infection.

Relatively weak co-existence of both swollen butt and markedly deteriorated crown was somewhat unexpected but, as indicated in Fig. 5. Either of the indicators separately with appropriate threshold values seems to be able to identify part of the diseased trees from healthy trees, but not all. This suggests that despite of the genetic similarity of the trees, there are differences in the dominant symptoms between the individuals. Genetic base of the tree will e.g. control the production of defensive chemicals such as phenolics and terpenoids, but resistance against fungal infection will depend on a range of external conditions as well, such as dominance of the respective tree, or availability of nutrients (Gibbs, 1967; Marčiulynas et al., 2020; Mukrimin et al., 2019; Piri, 2000). External factors as well as timing of getting infected may also affect the secretion of resinous compounds, which are likely to be a major cause for the measured swelling.

From a practical point of view, the presented TLS-based approach could be applied on two different levels. First, if a stand is suspected to be suffering from a *Heterobasidion* infection, the sample trees to be inspected in detail could be selected by the highest structural anomalies regarding to the point distribution patterns and the butt shape. And second, following a confirmed existence of root rot, the expectedly diseased trees could be objectively identified by applicable TLS-based thresholds which, together with tree and site characteristics of the stand, would assist in deciding suitable guidelines for management actions. This identification could potentially be improved by applying crown occupancy statistics and detecting spatial aggregations of expectedly diseased trees. As demonstrated in our classification test, combining different indicators will enable a relatively accurate

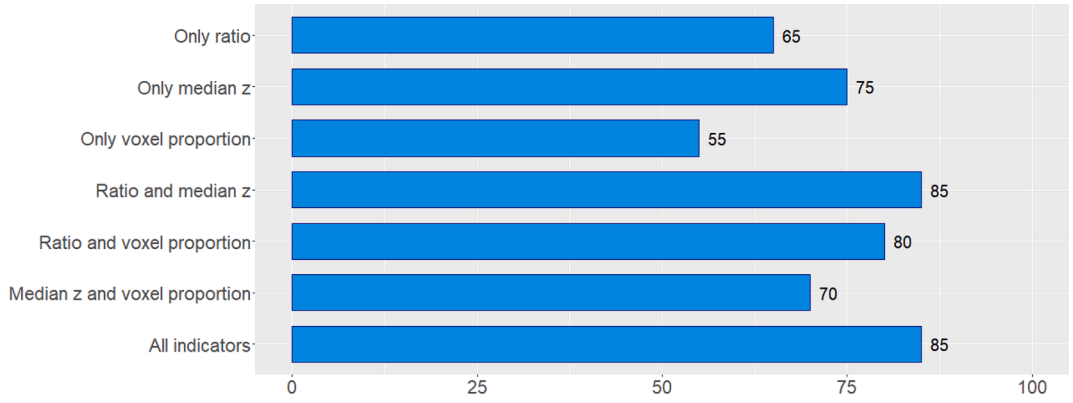

Fig. 6. Proportions (%) of correctly predicted infections with selected indicators and their combinations.

identification of the infection status, but more efforts should be targeted at finding their most applicable combinations. In addition to the studied structural characteristics, applying spectral information would provide additional assistance for detection, as chlorosis and browning of needles are known to be common root rot symptoms but not investigated in our study (Garbelotto and Gonthier, 2013; Kurkela, 2002).

The approach presented by us is based on scans made from fixed locations, which requires careful planning of the station locations and their spacing depending on the forest complexity, as well as substantial preparatory work at each station. In terms of operational applications, which should preferably be repeated at a few years' interval on susceptible locations, further development of the procedures should however be targeted on mobile scanners instead of static approaches. While the accuracy of mobile scanning systems is usually inferior compared to station-based and co-registered TLS data, they however have important advantages in terms of higher efficiency, lower operation costs, and reduction of occlusion effects (Bauwens et al., 2016; Bienert et al., 2018; Liang et al., 2016). The prevalence of occlusions at the lowest part of the stem is not always a problem, but when this is the case, their efficient removal is particularly crucial for accurate detection of stem dimensions. One potential platform of a mobile scanner would be a harvester, with consequent capabilities of e.g. assisted selective logging by prioritizing trees with deteriorated crowns. This would need highly automatized but reliable feature extraction and advanced on the fly processing solutions, which should be emphasized in further research.

5. Conclusions

We showed that TLS-derived data offers novel possibilities for detecting structural differences of Scots pines, which can be connected to Heterobasidion root rot infection. As such this has important implications for further applications but given the limited data from a single site applied in our research, additional studies on identifying the most applicable but simultaneously simple indicators, their thresholds and dependencies are needed. This information, together with efficient, automatized and accurate TLS processing, will improve our understanding of the root rot derived structural changes as well as enable developing operational applications to minimize the consequent losses.

CRediT authorship contribution statement

Timo P. Pitkänen: Formal analysis, Writing - original draft, Writing - review & editing. **Tuula Piri:** Investigation, Writing - original draft, Writing - review & editing. **Aleksi Lehtonen:** Conceptualization, Writing - review & editing, Supervision. **Mikko Peltoniemi:** Conceptualization, Investigation, Writing - review & editing.

Declaration of Competing Interest

The authors declare that they have no known competing financial interests or personal relationships that could have appeared to influence the work reported in this paper.

Acknowledgements

This work was supported by the Academy of Finland projects BiBiFe (no. 325680) and UNITE (no. 337655). Authors also wish to thank Ari Rajala, Timo Siitonen and Jukka Lehtimäki for efficient but careful fieldwork.

References

Alexander, S.A., et al., 1980. Association of Heterobasidion annosum and the Southern Pine Beetle on Loblolly Pine. Phytopathology 70, 510–513.
Asiegbu, F.O., Adomas, A., Stenlid, J., 2008. Conifer root and butt rot caused by Heterobasidion annosum (Fr.) Bref. s.l. Mol. Plant Pathol. 6, 395–409.
Azuan, N.H., et al., 2019. Analysis of changes in oil palm canopy architecture from basal stem rot using terrestrial laser scanner. Plant Dis. 103, 3218–3225.
Barbeito, I., et al., 2017. Terrestrial laser scanning reveals differences in crown structure of Fagus sylvatica in mixed vs. pure European forests. For. Ecol. Manage. 405, 381–390.
Bauwens, S., Bartholomeus, H., Calders, K., Lejeune, P., 2016. Forest inventory with terrestrial LiDAR: A comparison of static and hand-held mobile laser scanning. Forests 7, 127.
Bienert, A., et al., 2018. Comparison and combination of mobile and terrestrial laser scanning for natural forest inventories. Forests 395, 9.
Bonello, P., et al., 2008. Systemic effects of Heterobasidion annosum s.s. infection on severity of Diplodia pinea tip blight and terpenoid metabolism in Italian stone pine (Pinus pinea). Tree Physiol. 28, 1653–1660.
Boudon, F., et al., 2014. Quantitative assessment of automatic reconstructions of branching systems obtained from laser scanning. Ann. Bot. 114, 853–862.
Byler, J.W., 1989. Symptoms and Diagnosis of Annosus Root Disease in the Intermountain Western United States. In: Otrosina, W.J., Scharpf, R.W. (Eds.), Proceedings of the Symposium on Research and Management of Annosus Root Disease (Heterobasidion annosum) in Western North America. Pacific Southwest Forest and Range Experiment Station, Berkeley, pp. 37–39.
DeNitto, G.A., 1989. Characteristics of Annosus Root Disease in the Pacific Southwest. In: Otrosina, W.J., Scharpf, R.F. (Eds.), Proceedings of the Symposium on Research and Management of Annosus Root Disease (Heterobasidion annosum) in Western North America. Pacific Southwest Forest and Range Experiment Station, Berkeley, pp. 43–47.
Disney, M., et al., 2019. Innovations in ground and airborne technologies as reference and for training and validation: Terrestrial Laser Scanning (TLS). Surv. Geophys. 40, 937–958.
Eyles, A., et al., 2007. Cross-induction of systemic induced resistance between an insect and a fungal pathogen in Austrian pine over a fertility gradient. Oecologia 153, 365–374.
Garbelotto, M., Gonthier, P., 2013. Biology, epidemiology, and control of Heterobasidion Species worldwide. Annu. Rev. Phytopathol. 51, 39–59.
Gibbs, J.N., 1967. The role of host vigour in the susceptibility of pines to Fomes annosus. Ann. Bot. 31, 803–815.
Gonthier, P., Thor, M., 2013. Annosus root and butt rots. In: Gonthier, P., Nicolotti, G. (Eds.), Infectious Forest Diseases. CABI International, Wallingford, pp. 128–158.
Greig, B.J.W., 1998. Field recognition and diagnosis of Heterobasidion annosum. In: Woodward, S., Stenlid, J., Karjalainen, A. (Eds.), Heterobasidion annosum: Biology, Ecology, Impact, and Control. CAB International, Cambridge, pp. 35–41.
Greig, B.J.W., Pratt, J.E., 1976. Some observations on the longevity of Fomes annosus in conifer stumps. Forest Pathol. 6, 250–253.
Husin, N.A., et al., 2020. Application of ground-based LiDAR for analysing oil palm canopy properties on the occurrence of Basal Stem Rot (BSR) disease. Sci. Rep. 10, 6464.
Hynynen, J., Saramäki, J., 1995. Ensiharvennuksen viivästymisen ja harvennusvoimakkuuden vaikutus nuoren männikön kehitykseen. Folia Forestalia 99–113.
Jankowiak, R., Rossa, R., 2008. Associations between Pityogenes bidentatus and fungi in young managed Scots pine stands in Poland. Forest Pathol. 38, 169–177.
Johansson, S.M., Pratt, J.E., Asiegbu, F.O., 2002. Treatment of Norway spruce and Scots pine stumps with urea against the root and butt rot fungus Heterobasidion annosum - possible modes of action. For. Ecol. Manage. 157, 87–100.
Khosrokhani, M., Khairunniza-Bejo, S., Pradhan, B., 2018. Geospatial technologies for detection and monitoring of Ganoderma basal stem rot infection in oil palm plantations: a review on sensors and techniques. Geocarto International 33, 260–276.
Kolosova, N., Bohlmann, J., 2012. Conifer Defense Against Insects and Fungal Pathogens. In: Growth and Defence in Plants. Springer, Dordrecht, pp. 85–109.
Korhonen, K., 1978. Intersterility groups of Heterobasidion annosum. Communicationes Instituti Forestalis Fenniae 94. Finnish Forest Research Institute, Helsinki.
Kurkela, T., 2002. Crown Condition as an Indicator of the Incidence of Root Rot Caused by Heterobasidion annosum in Scots Pine Stands. Silva Fennica 36, 451–457.
Laasasenaho, J., 1982. Taper curve and volume functions for pine, spruce and birch. Finnish Forest Research Institute, Helsinki.
Laine, L., 1976. The Occurence of Heterobasidion annosum (Fr.) Bref. in Woody Plants in Finland. Finnish Forest Research Institute, Helsinki.
Liang, X., et al., 2016. Terrestrial laser scanning in forest inventories. ISPRS J. Photogramm. Remote Sens. 115, 63–77.
Li, Y., et al., 2020. Retrieval of tree branch architecture attributes from terrestrial laser scan data using a Laplacian algorithm. Agric. For. Meteorol. 284, 107874.
Lygis, V., Vasiliauskas, R., Stenlid, J., 2004. Planting Betula pendula on pine sites infested by Heterobasidion annosum: disease transfer, silvicultural evaluation, and community of wood-inhabiting fungi. Can. J. For. Res. 34, 120–130.
Malhi, Y., et al., 2018. New perspectives on the ecology of tree structure and tree communities through terrestrial laser scanning. Interface Focus 8, 20170052.
Marčiulynas, A., et al., 2020. Resistance of Scots pine half-sib families to Heterobasidion annosum in progeny field trials. Silva Fennica 54, 10276.
Martin-Ducup, O., Schneider, R., Fournier, R.A., 2016. Response of sugar maple (Acer saccharum, Marsh.) tree crown structure to competition in pure versus mixed stands. For. Ecol. Manage. 374, 20–32.
Metz, J., et al., 2013. Crown modeling by terrestrial laser scanning as an approach to assess the effect of aboveground intra- and interspecific competition on tree growth. For. Ecol. Manage. 310, 275–288.

Mukrimin, M., et al., 2019. Evaluation of potential genetic and chemical markers for Scots pine tolerance against Heterobasidion annosum infection. Planta 250, 1881–1895.
Nicolotti, G., Gonthier, P., Varese, G.C., 1999. Effectiveness of some biocontrol and chemical treatments against Heterobasidion annosum on Norway spruce stumps. Eur. J. For. Pathol. 29, 339–346.
Olofsson, K., Holmgren, J., 2016. Single tree stem profile detection using terrestrial laser scanner data, flatness saliency features and curvature properties. Forests 7, 207.
Perttunen, J., Sievänen, R., Piri, T., Kalliokoski, T., 2013. Modelling the colonization of the decay fungus Heterobasidion annosum in Scots pine (Pinus sylvestris L.) root system. In: Saariselkä, Finland, Proceedings of the 7th International Conference on Functional-Structural Plant Models.
Otrosina, W.J., et al., 1997. Blue-stain Fungi Associated with Roots of Southern Pine Trees Attacked by the Southern Pine Beetle, Dendroctonus frontalis. Plant Dis. 81, 942–945.
Piri, T., 2000. Response of compensatory-fertilized Pinus sylvestris to infection by Heterobasidion annosum. Scandinavian J. Forest Res. 15, 218–224.
Piri, T., 2003. Early development of root rot in young Norway spruce planted on sites infected by Heterobasidion in southern Finland. Can. J. For. Res. 33, 604–611.
Pitkänen, T.P., Raumonen, P., Kangas, A., 2019. Measuring stem diameters with TLS in boreal forests by complementary fitting procedure. ISPRS J. Photogramm. Remote Sens. 147, 294–306.
Puletti, N., Grotti, M., Scotti, R., 2019. Evaluating the Eccentricities of Poplar Stem Profiles with Terrestrial Laser Scanning. Forests 10, 239.
Pyörälä, J., et al., 2018. Assessing branching structure for biomass and wood quality estimation using terrestrial laser scanning point clouds. Can. J. Remote Sens. 44, 462–475.
Ruotsalainen, S., 2014. Increased forest production through forest tree breeding. Scand. J. For. Res. 29, 333–344.
Rönnberg, J., Petrylaite, E., Nilsson, G., Pratt, J., 2006. Two studies to assess the risk to Pinus sylvestris from Heterobasidion spp. in southern Sweden. Scand. J. For. Res. 21, 405–413.
Saarinen, N., et al., 2017. Feasibility of Terrestrial laser scanning for collecting stem volume information from single trees. ISPRS J. Photogramm. Remote Sens. 123, 140–158.
Seidel, D., et al., 2015. How neighborhood affects tree diameter increment – New insights from terrestrial laser scanning and some methodical considerations. For. Ecol. Manage. 336, 119–128.
Seidel, D., Leuschner, C., Müller, A., Krause, B., 2011. Crown plasticity in mixed forests—Quantifying asymmetry as a measure of competition using terrestrial laser scanning. For. Ecol. Manage. 261, 2123–2132.
Swedjemark, G., Stenlid, J., 1995. Susceptibility of conifer and broadleaf seedlings to Swedish S and P strains of Heterobasidion annosum. Plant. Pathol. 44, 73–79.
Van Laar, A., Akça, A., 2007. Forest Mensuration. Springer, Dordrecth.
Wang, L., et al., 2014. Incidence and impact of root infection by Heterobasidion spp., and the justification for preventative silvicultural measures on Scots pine trees: A case study in southern Sweden. For. Ecol. Manage. 315, 153–159.
Varese, G.C., Gonthier, P., Nicolotti, G., 2003. Long-term effects on other fungi are studied in biological and chemical stump treatments in the fight against Heterobasidion annosum coll. Mycologia 95, 379–387.
Werner, A., Łakomy, P., 2002. Intraspecific variation in Heterobasidion annosum for mortality rate on Pinus sylvestris and Picea abies seedlings grown in pure culture. Mycologia 94, 856–861.
Woodward, S., Stenlid, J., Karjalainen, R., Hüttermann, A., 1998. Heterobasidion annosum: Biology, Ecology, Impact, and Control. CABI Publishing, Wallingford.
Zaļuma, A., et al., 2019. Infection and spread of root rot caused by Heterobasidion spp. in Pinus contorta plantations in Northern Europe: three case studies. Can. J. For. Res. 49, 969–977.